SUPPORTING INFORMATION

Improved Electrocatalytic Water Splitting Reaction on CeO_2(111) by Strain Engineering: A DFT+U Study

Tiantian Wu, Tejs Vegge and Heine Anton Hansen*

Department of Energy Conversion and Storage, Technical University of Denmark, Fysikvej, 2800 Kgs. Lyngby, Denmark.

*Corresponding author:

Assoc. Prof. Dr. Heine Anton Hansen   E-mail: heih@dtu.dk   Tel: +45 45258211

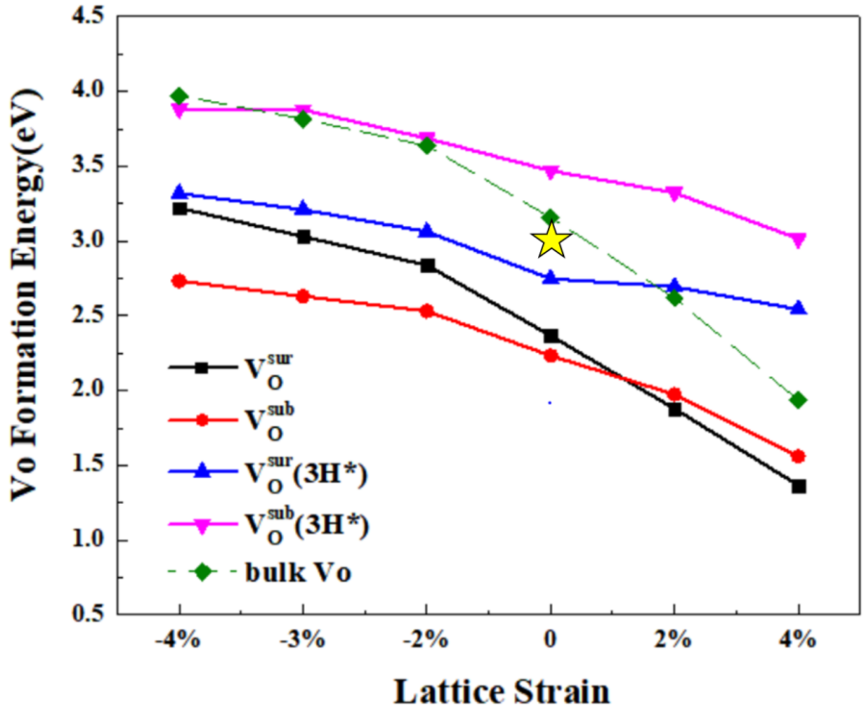

Figure S1. Formation energy of an oxygen vacancy as a function of lattice strain compared to the vacancy formation in bulk ceria. Yellow star represents the vacancy formation energy for unstrained bulk ceria reported by Gopal et al [1]. For creating an oxygen vacancy in unstrained ceria, we have compared the different Ce^{3+} locations in ceria. The most stable configuration of V_O^{sub} has $2Ce^{3+}$ next nearest neighbored to it, which is about 0.5 eV more stable than that $2Ce^{3+}$ locates nearest-neighbored to the V_O^{sub}, as shown in Table S8. For V_O^{sur}, the next nearest neighbored locations of Ce^{3+} is 0.18 eV more favored over the nearest-neighbored locations as shown in Table S9. These findings agree well with the results reported by Ganduglia-Pirovano et al.[2] By comparison, we have investigated the different Ce^{3+} locations at -4%, -3% -2%, 2%, and 4% strain as shown in Tables S8 and S9. The preference of Ce^{3+} locations for both V_O^{sub} and V_O^{sur} is not affected by strain, which is consistent with Ma's findings[3]. For each vacancy formation, the energy difference between different Ce^{3+} locations is below 0.5 eV and the reported polaron hopping between different Ce^{3+} locations is facile[4,5]. In addition, vacancy formation and diffusion is not fundamental step to the discussions on the efficient reaction pathway or TOF as shown in Figure 5 and 6 in the manuscript. Herein, all Ce^{3+} locations are nearest-neighbored to an oxygen vacancy or hydroxyls.

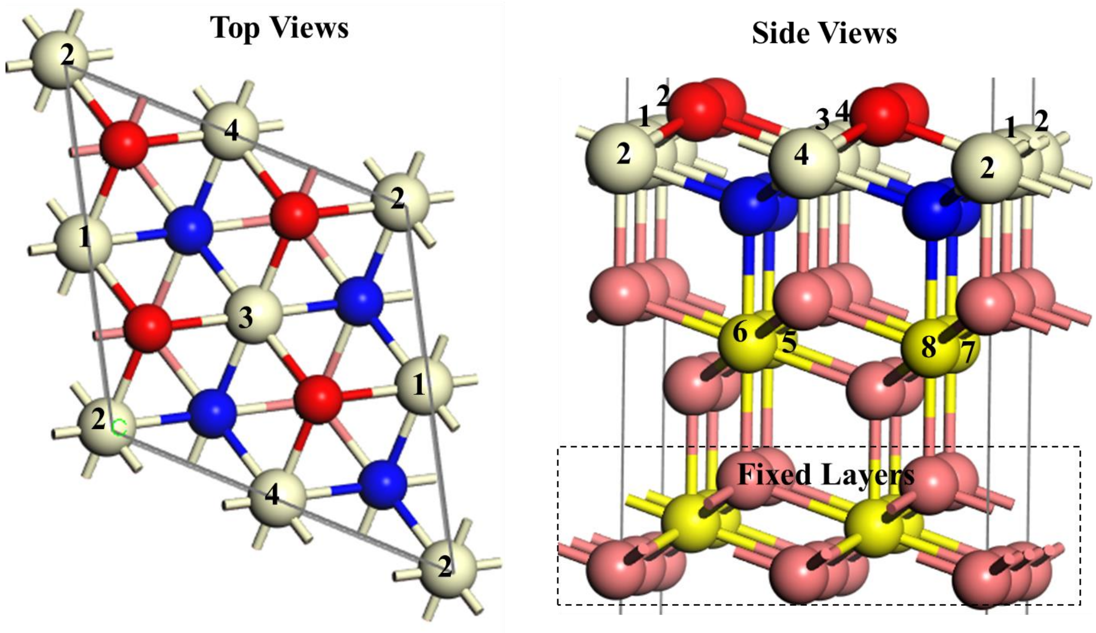

Figure S2. The top and side views of labelled cerium atoms with atom numbers in the top and subsurface layers of CeO_2(111). Color legend is the same as shown in Figure 1.

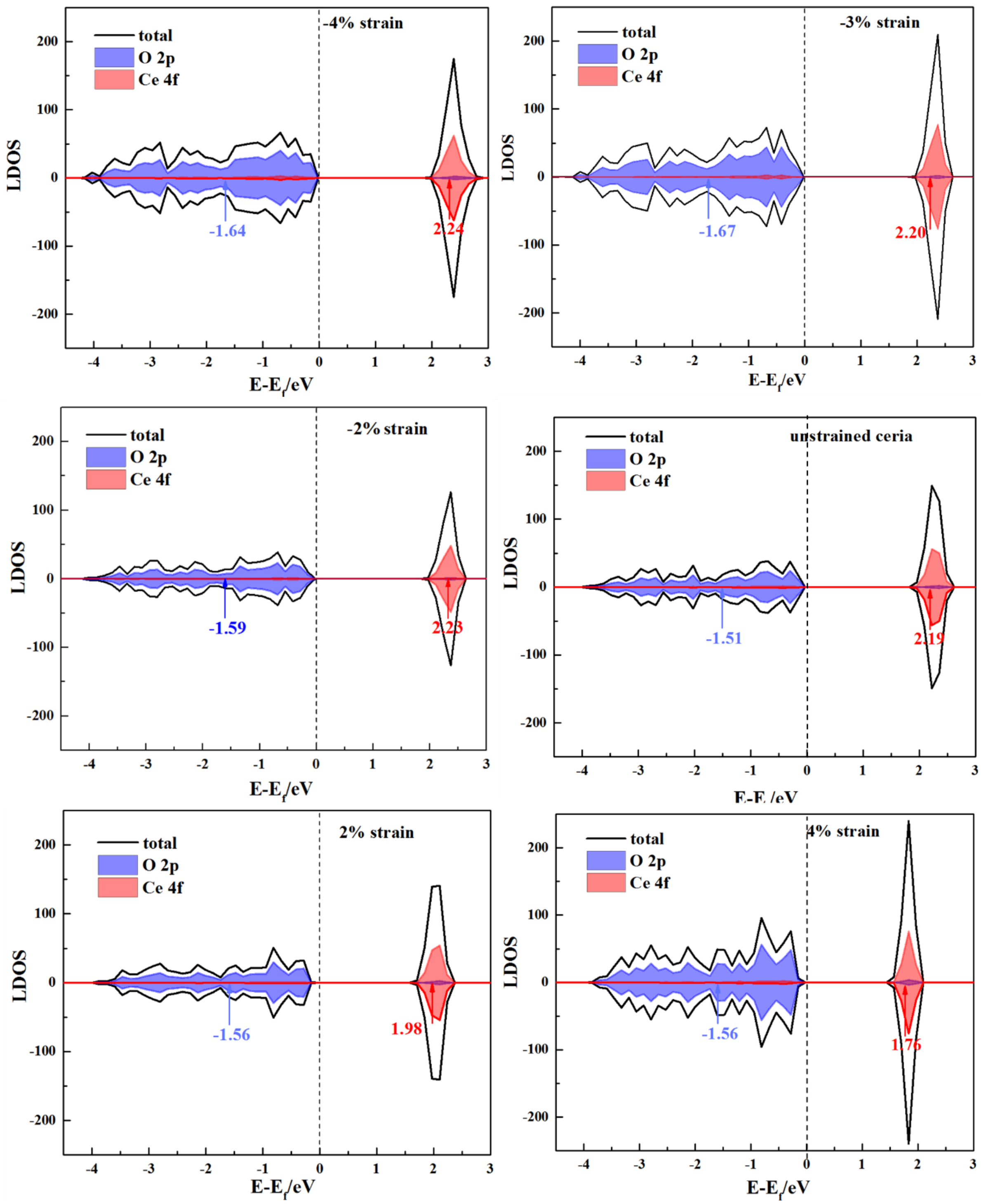

Figure S3. Spin-polarized density of states projected on O 2p and Ce 4f orbitals of strained and unstrained $CeO_2(111)$. The O 2p and Ce 4f band centers are,labeled and marked by blue and red arrows, respectively. The Fermi level is set to zero. The density of states are calculated using a Γ-centered 13×13×1 k-point mesh.

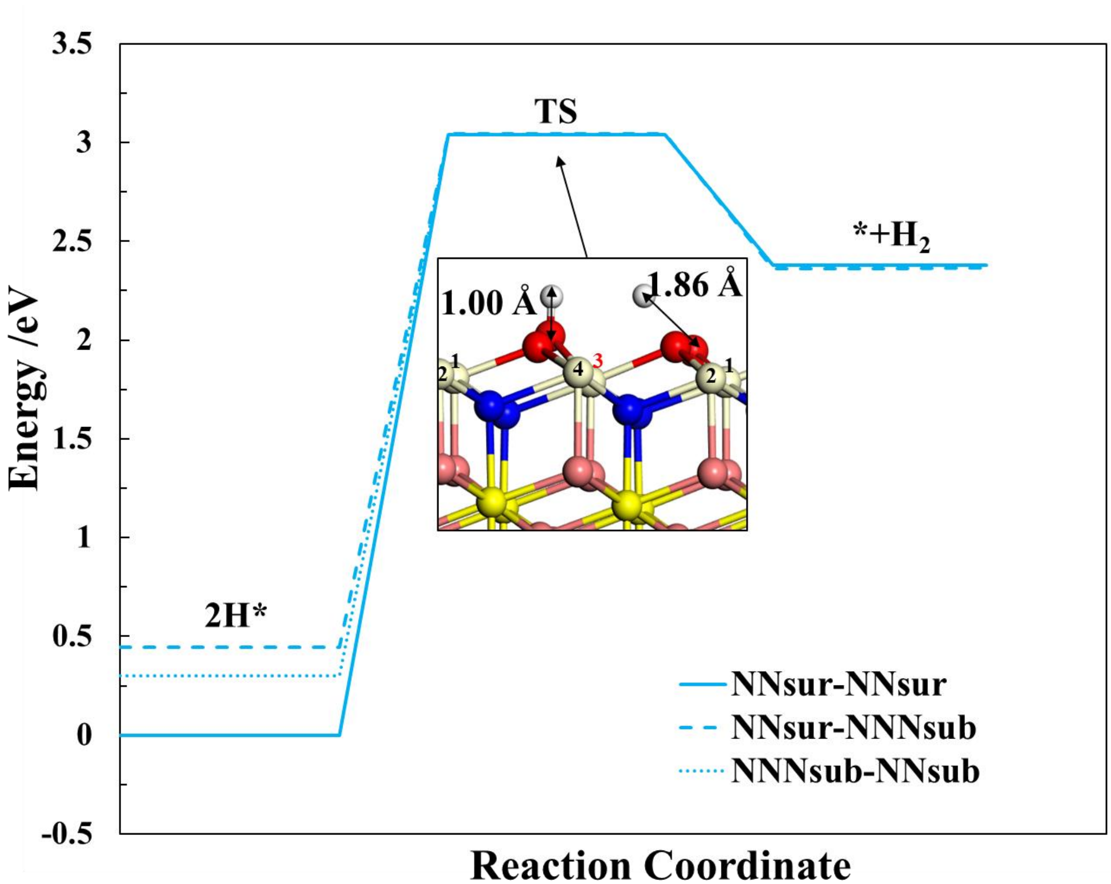

Figure S4. Hydroxyl decomposition into H_2 on the 2H* with the most favorable Ce^{3+} locations of NN_{sur}-NN_{sur}, compared to Ce^{3+} locations of NN_{sur}-NNN_{sub} and NNN_{sub}-NN_{sub}. We found the same transition sate (TS) for H_2 formation on the 2H* with different Ce^{3+} locations, where one H moves close to the other H leading to the breaking of one O-H. At the TS, there is only one Ce^{3+} locating at number 3 cerium as labelled in Figure S4. The configurations of 2H* and *+H_2 are present in Figure 2 in the manuscript. For further description of the Ce^{3+} locations refer to Figure S2 and Table S2.

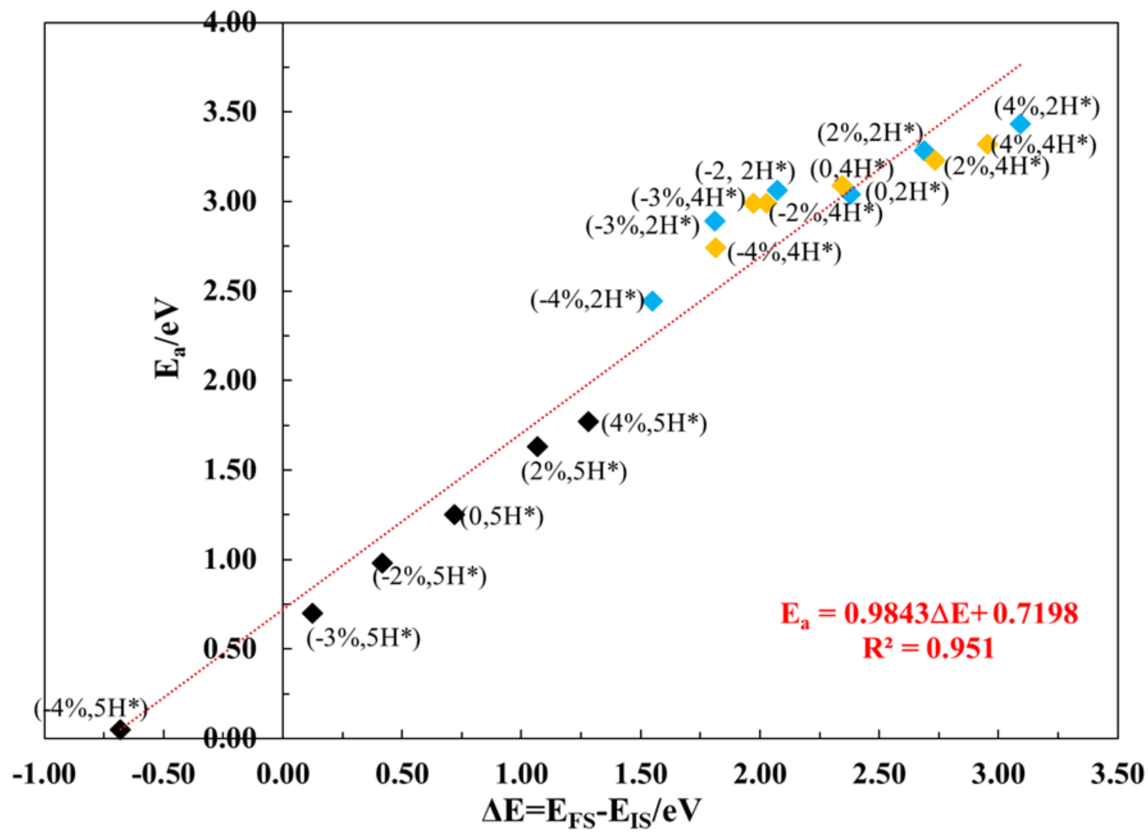

Figure S5. Brønsted-Evans-Polanyi (BEP) scaling relationships for the hydroxyl decomposition to form hydrogen on the different hydroxylated $CeO_2(111)$ surfaces with different strain. The annotation (-4%, 5H*) indicates the activation energy is calculated for a $CeO_2(111)$ surface under -4 % strain and adsorbed with 5H.

Descriptors for E_a

"Seven pillars" describing the geometric and electronic properties, has been proposed to contribute to the selectivity in the heterogeneous oxidation catalysis.[6] Capdevila-Cortada et al. [7] successfully developed the descriptor analysis in methanol conversion on doped $CeO_2(111)$. Inspired by these investigations, we assess the following geometric and electronic descriptors:

(1) Geometric descriptors:

  (a) The lattice parameter, a, which is directly affected by strain and can be experimentally measured from the XRD[8].

(b) The Ce-O distance, $r_{Ce\text{-}O}$, turns out ot be linearly dependent on the lattice parameter as shown in Figure S6. Thus, we only consider lattice parameter as the geometric descriptor in this study.

(2) Electronic descriptors:

(a) The basicity of lattice oxygen which is obtained using the O (2p) band center $\varepsilon_{O(2p)}$. In addition, Ce (4f) band center, $\varepsilon_{Ce(4f)}$, is also used to describe the electron localization on Ce 4f states and redox ability of CeO_2(111). The basicity can be experimentally assessed by studying the adsorption of the CO or NH_3 using FTIR spectroscopy[9].

(b) The redox character, E_{red}, which is the energy for reduction of one Ce^{4+} to Ce^{3+}. Temperature-programmed reduction (TPR) or isotopic exchange can directly give information on the redox character[7]. The reduction energy is by the reduction reaction $CeO_2 \rightarrow Ce_2O_3 + {}^1/_2\, O_2$.

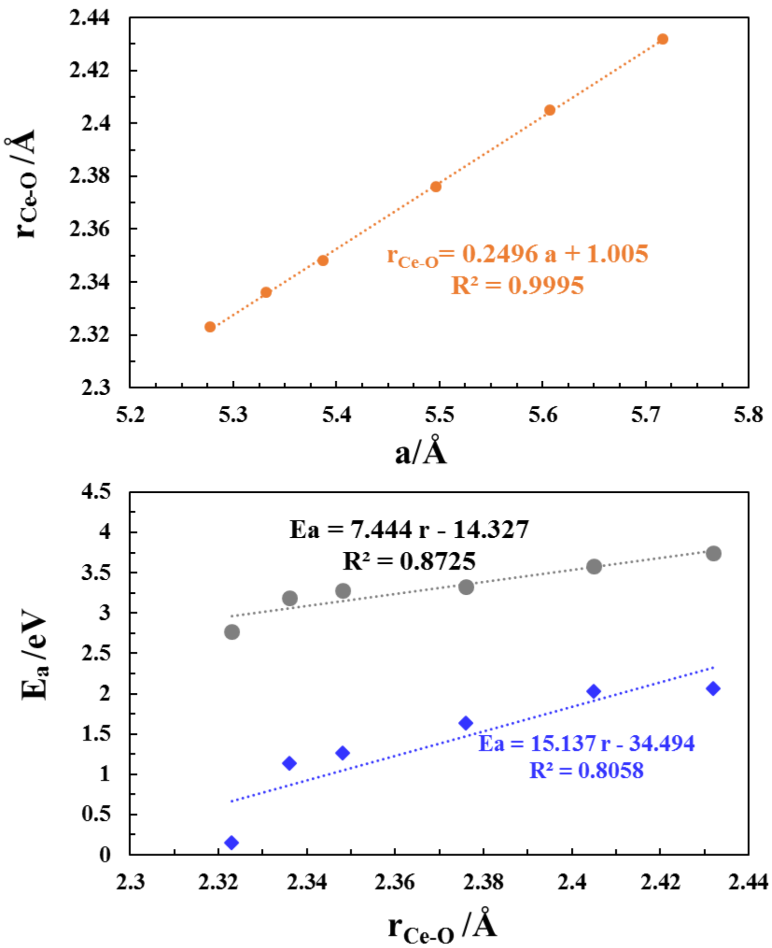

Figure S6. Top: the Ce-O distance, $r_{Ce\text{-}O}$, depends linearly on the bulk lattice parameter, a. Bottom: E_a versus the Ce-O distance for hydroxyl decomposition on the partially (gray spheres) and excessively hydroxylated (blue diamonds) surface.

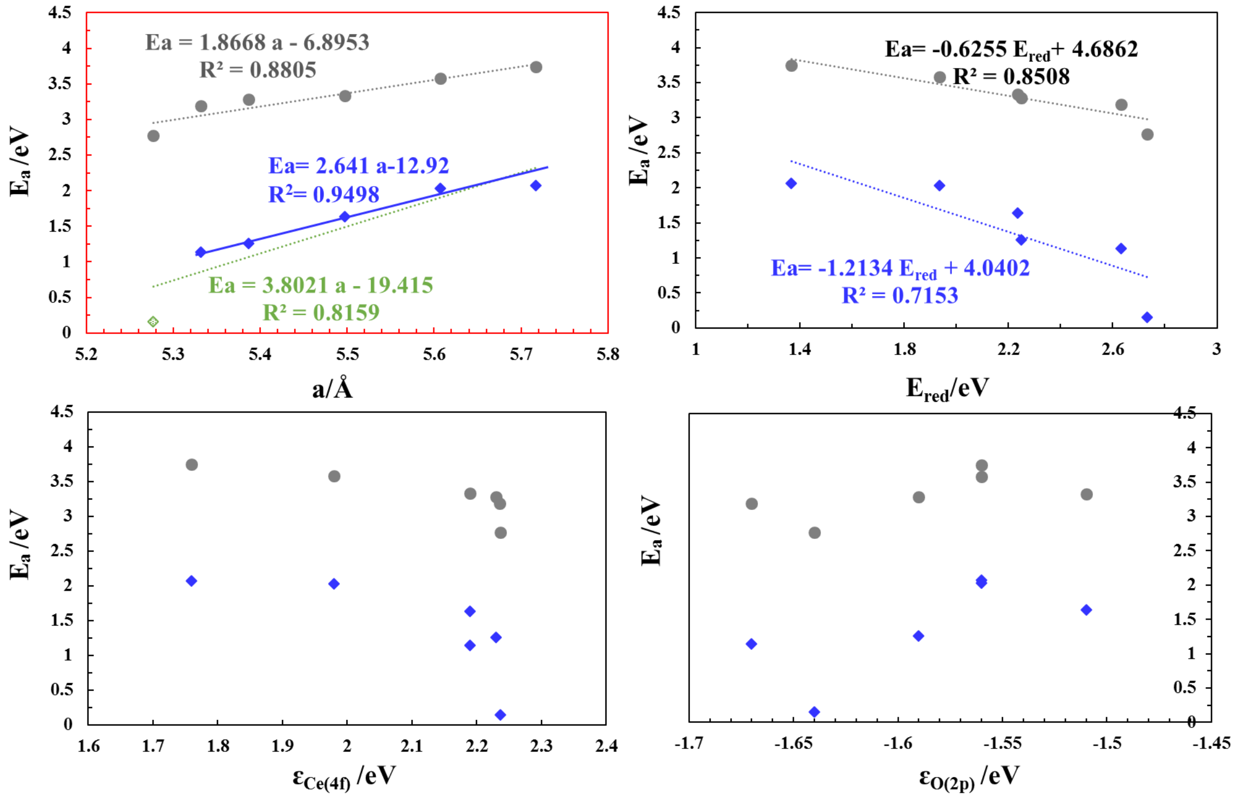

Figure S7. Activation energy for hydroxyl decomposition as a function of the lattice parameter, a, the reduction energy, E_{red}, the Ce 4f band center, $\varepsilon_{Ce(4f)}$, or O 2p band center, $\varepsilon_{O(2p)}$. The reactions on partially and excessively hydroxylated CeO_2(111) are marked, respectively, in grey and blue. The green line shows the scaling between E_a and a (including the data under -4% strain).

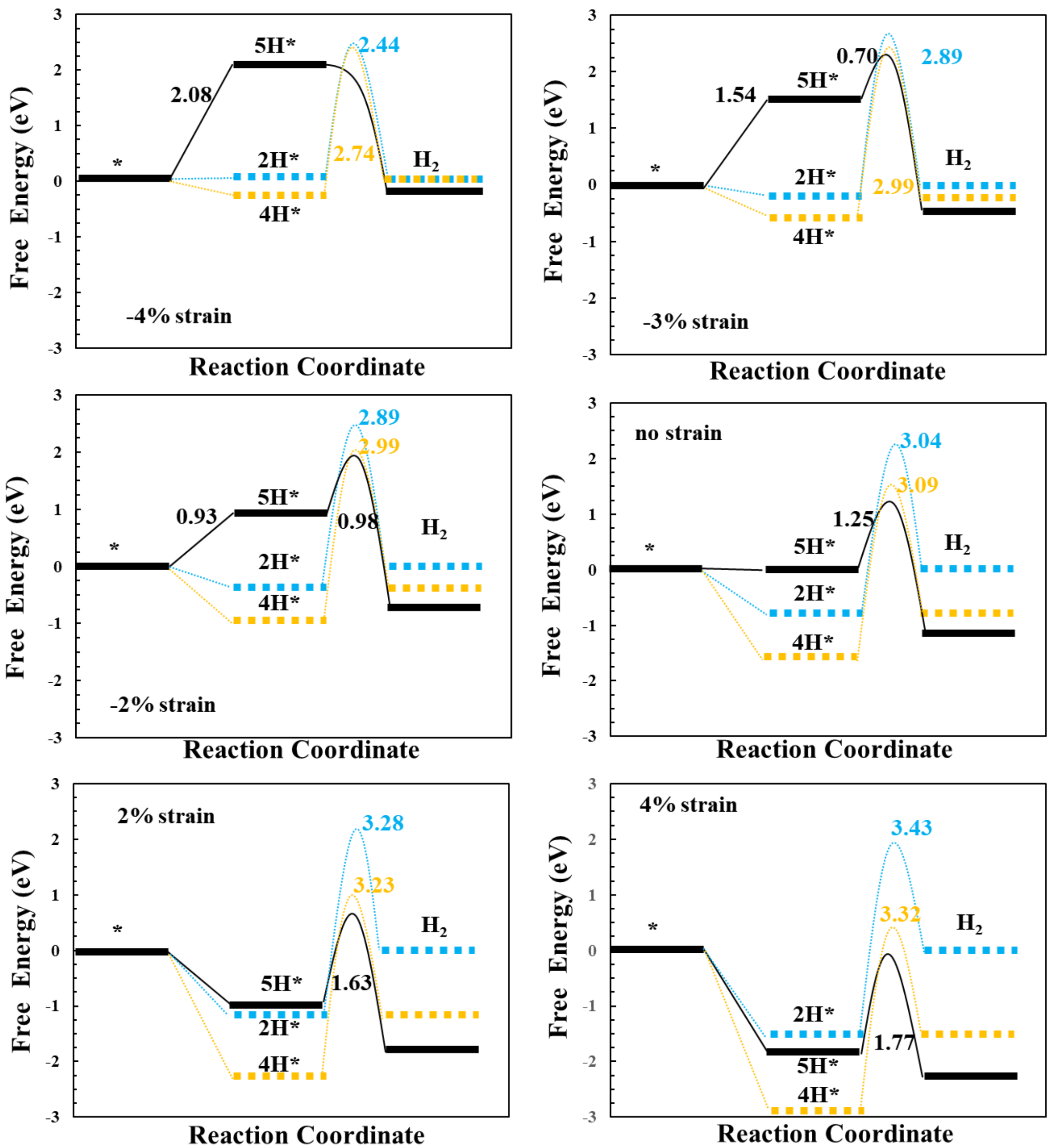

Figure S8. Simplified free energy diagrams for hydroxyl decomposition on the partially (2H*), fully (4H*) and excessively (5H*) hydroxylated $CeO_2(111)$ under different strain at 1000 K. A solid line highlights the most efficient reaction pathway at each lattice strain.

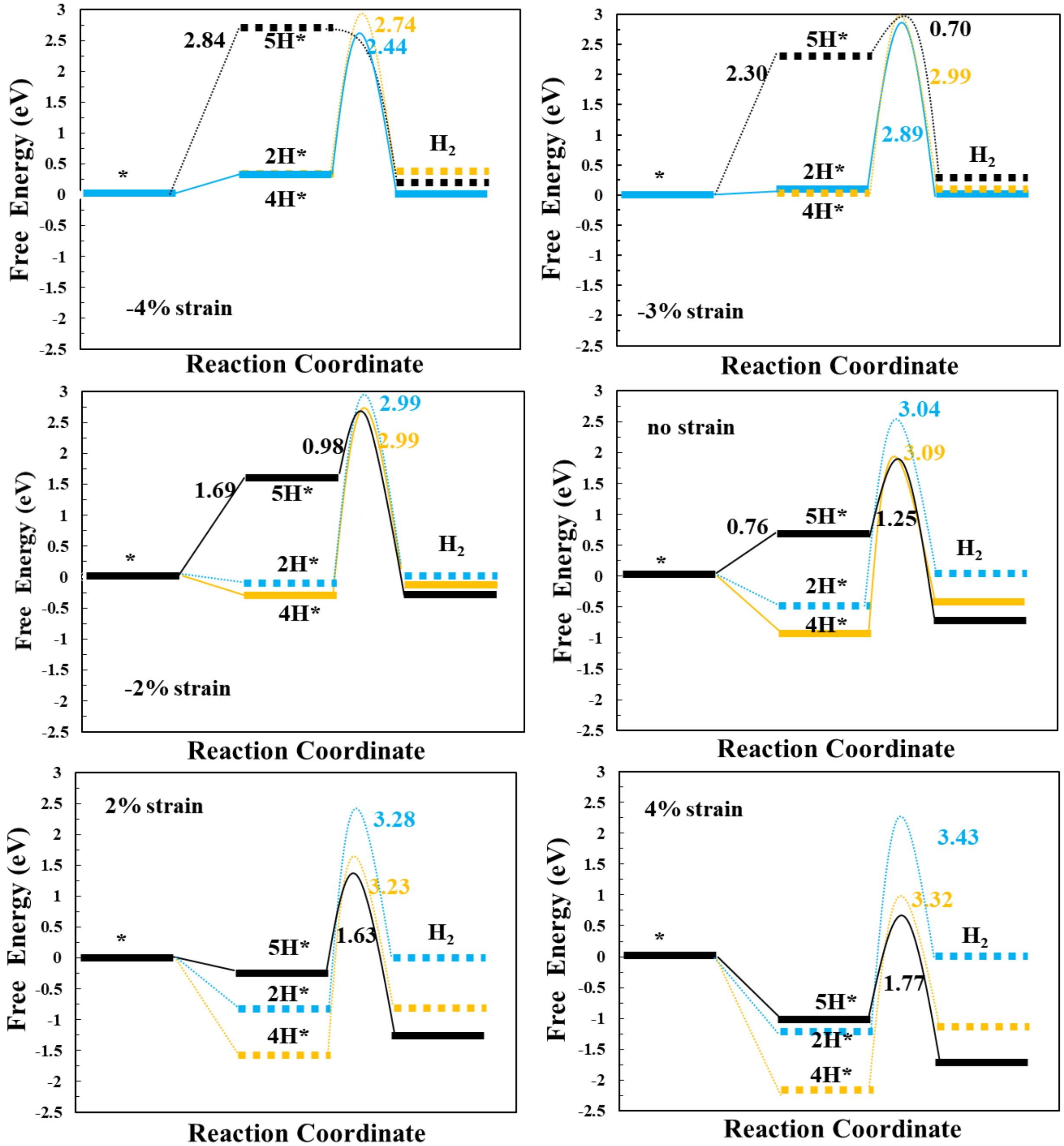

Figure S9. Simplified free energy diagrams for hydroxyl decomposition on partially (2H*), fully (4H*) and highly (5H*) hydroxylated CeO_2(111) under different strain at 1200 K. A solid line highlights the most efficient reaction pathway at each lattice strain.

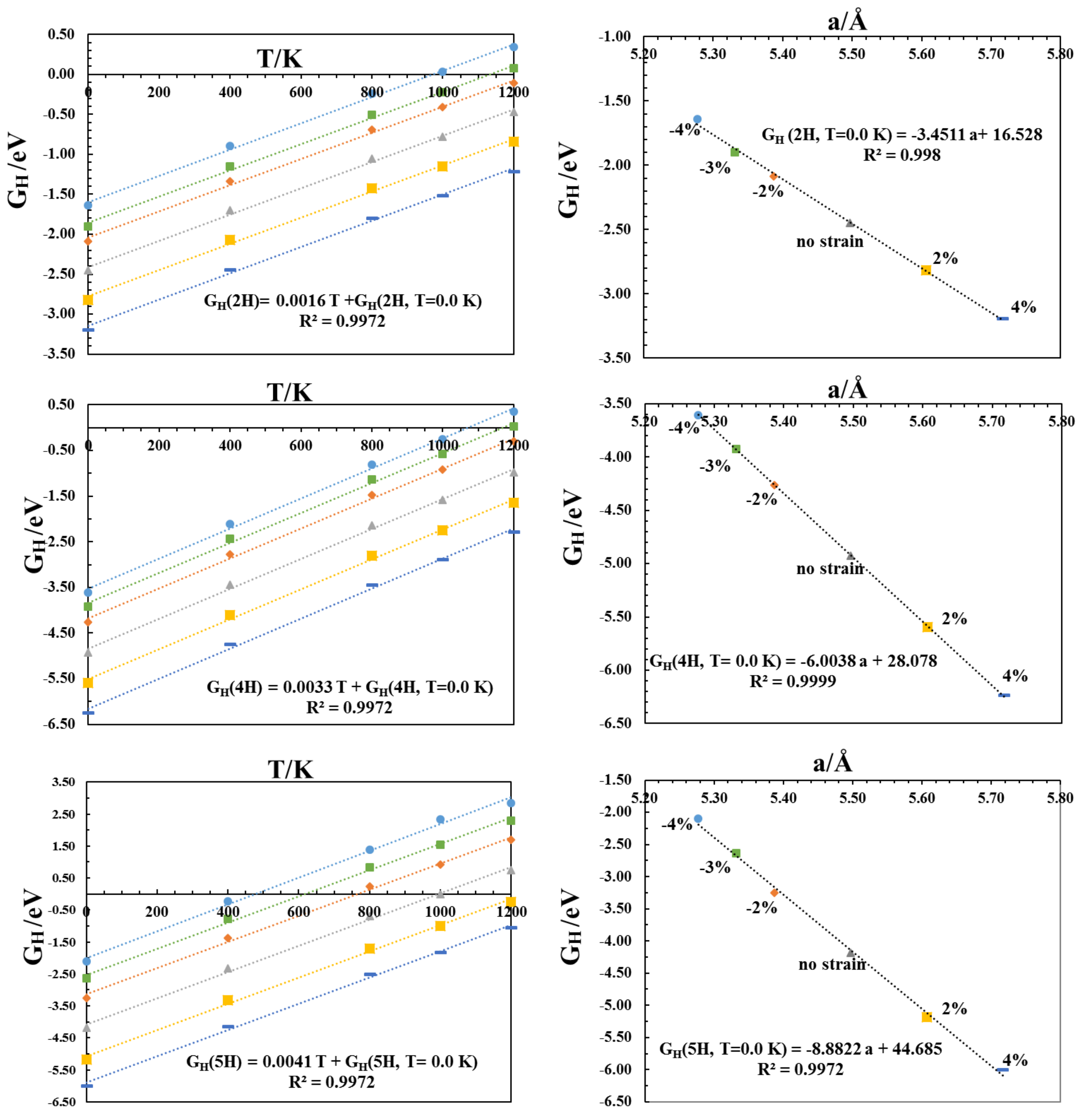

Figure S10. Free energy of partially (2H*), fully (4H*) and excessively (5H*) hydroxylated CeO_2(111) as a function of temperature and lattice parameter. We find a linear scaling between the operating temperature and the free energy of hydroxylated CeO_2(111) surfaces such as 2H*, 4H* and 5H*. The free energy of 2H*, 4H* and 5H* can be fitted by experimentally measurable descriptors such as temperature (T) and the lattice parameter (a) as follows:

$$G_H(2H) = 0.0016T - 3.4511a + 16.5280$$

$$G_H(4H) = 0.0033T - 6.0038a + 28.0780$$

$$G_H(5H) = 0.0041T - 8.8822a + 44.6850$$

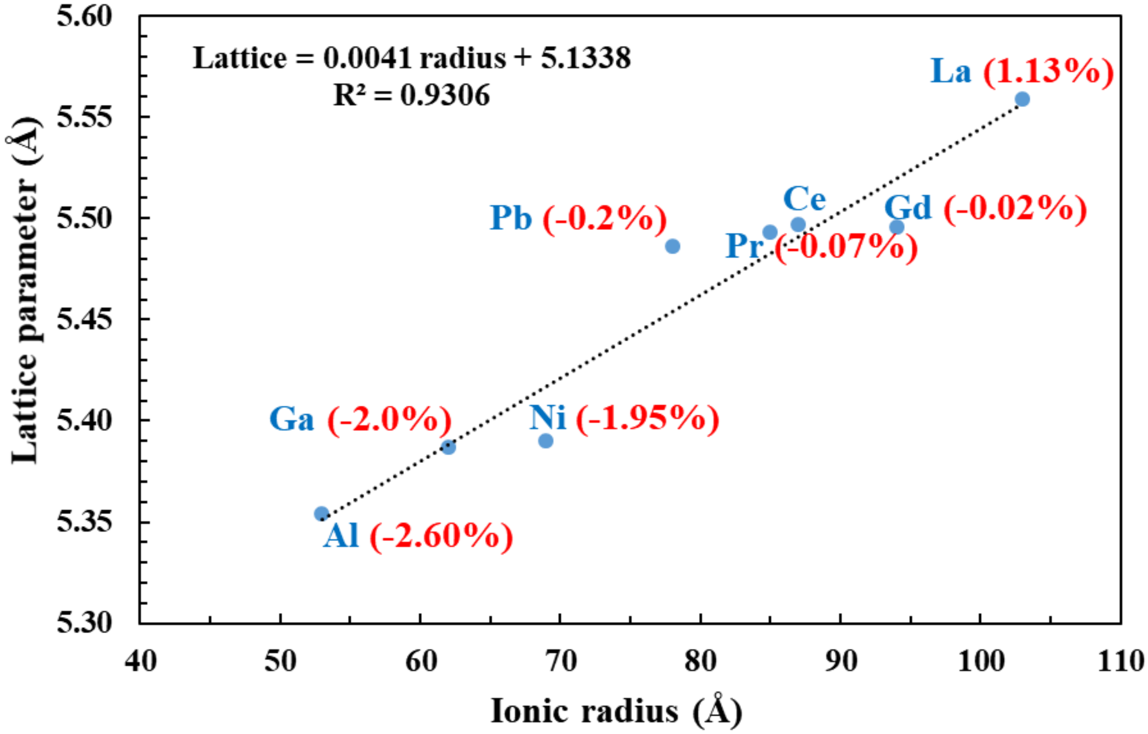

Figure S11. Calculated lattice parameter of doped bulk ceria as a function of the dopant ionic radius. Numbers in parentheses denote the strain of undoped ceria with the same lattice parameter as the doped ceria.

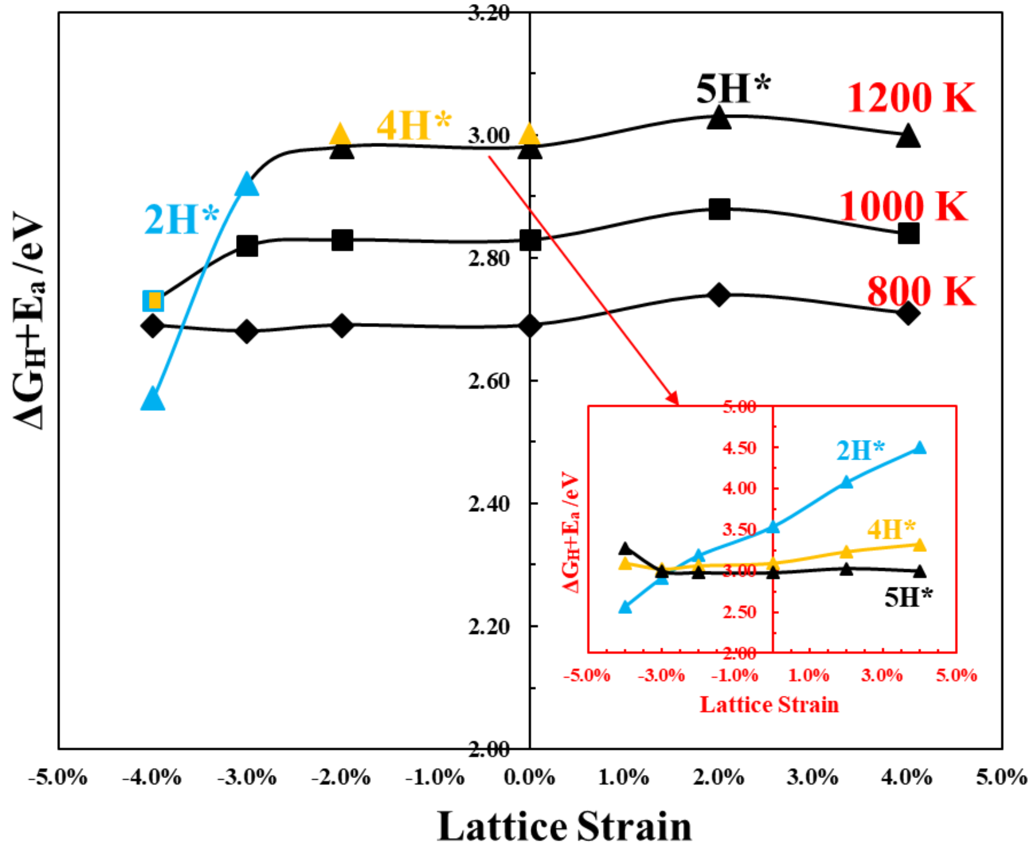

Figure S12. Free energy span, ΔG_H+Ea, for the most efficient WSR pathway versus strain at different temperatures. The free energy span for WSR pathways on the partially (2H*), fully (4H*), and excessively (5H*) hydroxylated CeO_2(111) at 1200 K is shown in the inset.

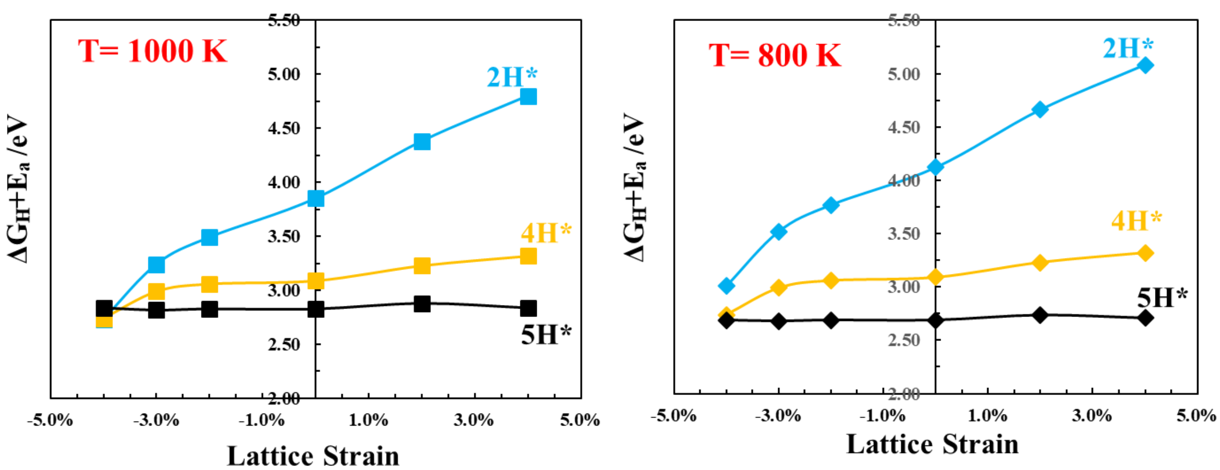

Figure S13. The free energy span for WSR pathways on the partially (2H*), fully (4H*), and excessively (5H*) hydroxylated CeO_2(111) at 800 and 1000 K.

Table S1. Lattice parameter, Ce-O bond length, O 2p $\varepsilon_{O(2p)}$ and Ce 4f $\varepsilon_{Ce(4f)}$ band centers of strained CeO_2(111). The centers of the O 2p and Ce 4f bands are referenced to the Fermi level.

This work	a (Å)	$r_{Ce\text{-}O}$ (Å)	$\varepsilon_{O(2p)}$ (eV)	$\varepsilon_{Ce(4f)}$ (eV)
CeO_2	5.497	2.376	-1.51	2.19
+4%	5.717	2.432	-1.56	1.76
+2%	5.607	2.405	-1.56	1.98
-2%	5.387	2.348	-1.59	2.23
-3%	5.332	2.336	-1.67	2.20
-4%	5.277	2.323	-1.64	2.24
Marcel's work[6]	a (Å)	$r_{Ce\text{-}O}$ (Å)		
CeO_2	5.497	2.375		
+2%	5.607	2.404		
-2%	5.387	2.348		

Table S2. The locations (atomic numbers) of Ce^{3+} states during pathways for the hydrogen production on ***partially (2H*), fully (4H*)*** and ***excessively (5H*)*** hydroxylated CeO_2(111), under different strain. All Ce^{3+} states are nearest-neighbored to an oxygen vacancy or hydroxyls. Atom numbering refers to Figure S2. The configurations of each intermediates are shown in Figure 2.

Strain	*******	***Vo^{sub}***	***TS1***	***Vo^{sur}***	***+H_2O_{ads}***	***TS2***	***2H****	***TS3***	****+H_2***
-4%		(1,3)	(1,3)	(2,4)	(2,4)		(3,4)	(4)	
-3%		(1,3)	(2,4)	(2,4)	(2,4)		(3,4)	(4)	
-2%		(1,3)	(2,4)	(2,4)	(2,4)		(1,2)	(2)	
0%		(1,3)	(1,3)	(2,4)	(2,4)		(2,3)	(3)	
2%		(1,3)	(1,3)	(2,4)	(2.4)		(2,4)	(2)	
4%		(1,3)	(2,4)	(2,4)	(2,4)		(1,2)	(2)	
Strain	***3H****	***3H*+Vo^{sub}***	***TS1'***	***3H*+Vo^{sur}***	***+H_2O_{ads}***	***TS2'***	***4H****	***TS3'***	***2H*+H_2***
-4%	(1,3,4)	(1,2,3,4,7)		(1,2,3,4,7)	(1,2,3,4,8)		(1,2,3,4)	(2,3,4)	(3,4)
-3%	(2,3,4)	(1,2,3,4,7)		(1,2,3,4,6)	(1,2,3,4,7)		(1,2,3,4)	(2,3,4)	(3,4)
-2%	(1,2,4)	(1,2,3,4,6)		(1,2,3,4,6)	(1,2,3,4,6)		(1,2,3,4)	(1,3,4)	(1,3)
0%	(1,2,3)	(1,2,3,4,7)		(1,2,3,4,8)	(1,2,3,4,8)		(1,2,3,4)	(1,2,3)	(1,3)
2%	(1,3,4)	(1,2,3,4,6)		(1,2,3,4,6)	(1,2,3,4,6)		(1,2,3,4)	(1,2,4)	(1,2)
4%	(1,2,4)	(1,2,3,4,5)		(1,2,3,4,7)	(1,2,3,4,7)		(1,2,3,4)	(1,2,4)	(1,2)
Strain	***3H****	***3H*+Vo^{sub}***	***TS1'***	***3H*+Vo^{sur}***	***+H_2O_{ads}***	***TS2''***	***5H****	***TS3''***	***3H*+H_2***
-4%	(1,3,4)	(1,2,3,4,7)		(1,2,3,4,7)	(1,2,3,4,8)	(1,2,3,4)	(1,2,4)		(1,3,4)
-3%	(2,3,4)	(1,2,3,4,7)		(1,2,3,4,6)	(1,2,3,4,7)		(1,2,3,4,7)	(1,2,3,4)	(2,3,4)
-2%	(1,2,4)	(1,2,3,4,6)		(1,2,3,4,6)	(1,2,3,4,6)		(1,2,3,4,7)	(1,2,3,4)	(1,2,4)
0%	(1,2,3)	(1,2,3,4,7)		(1,2,3,4,8)	(1,2,3,4,8)		(1,2,3,4,7)	(1,2,3,4)	(1,2,3)
2%	(1,3,4)	(1,2,3,4,6)		(1,2,3,4,6)	(1,2,3,4,6)		(1,2,3,4,7)	(1,2,3,4)	(1,2,4)
4%	(1,2,4)	(1,2,3,4,5)		(1,2,3,4,7)	(1,2,3,4,7)		(1,2,3,4,7)	(1,2,3,4)	(2,3,4)

Table S3. Adsorption energy of 2H with different Ce^{3+} locations (atom numbers) on unstrained ceria. Atom numbering refers to Figure S2. NNN and NN represent Ce^{3+} locating next nearest neighbor and nearest neighbor to hydroxyls, respectively. The subscripts of "sur" and "sub" represent Ce^{3+} locating in the top surface and subsurface, respectively.

Ce^{3+} locations to the Vo^{sur}	Atomic number of Ce^{3+}	E(2H)
NN_{sur}-NN_{sur}	(2,3)	-2.45
NNN_{sub}-NN_{sub}	(5,7)	-2.15
NN_{sur}-NNN_{sub}	(2,7)	-2.01

Table S4. Free energies of reduced states during pathways for the hydrogen production on ***partially (2H*), fully (4H*)*** and ***excessively (5H*)*** hydroxylated CeO_2(111), under different strain at 800 K.

Strain	*******	***Vo^{sub}***	***TS1***	***Vo^{sur}***	***$+H_2O_{ads}$***	***TS2***	***2H****	***TS3***	***$*+H_2$***
-4%	0.00	0.20	1.37	0.69	1.06		-0.24	2.20	0.00
-3%	0.00	0.10	0.78	0.50	0.87		-0.50	2.39	0.00
-2%	0.00	0.08	0.77	0.31	0.64		-0.69	2.30	0.00
0%	0.00	-0.29	0.55	-0.16	0.26		-1.06	1.98	0.00
2%	0.00	-0.59	0.03	-0.65	-0.12		-1.43	1.85	0.00
4%	0.00	-0.70	-0.54	-1.16	-0.44		-1.79	1.64	0.00
Strain	***3H****	***$3H*+Vo^{sub}$***	***TS1'***	***$3H*+Vo^{sur}$***	***$+H_2O_{ads}$***	***TS2'***	***4H****	***TS3'***	***$2H*+H_2$***
-4%	-0.54	0.81		0.25	0.88		-0.81	1.93	-0.24
-3%	-0.56	0.37		0.12	0.58		-1.14	1.85	-0.50
-2%	-1.08	0.08		-0.55	0.18		-1.47	1.52	-0.69
0%	-1.60	-0.66		-1.38	-0.53		-2.14	0.95	-1.06
2%	-2.05	-1.26		-1.89	-1.44		-2.80	0.43	-1.43
4%	-2.69	-2.21		-2.68	-2.18		-3.45	-0.13	-1.79
Strain	***3H****	***$3H*+Vo^{sub}$***	***TS1'***	***$3H*+Vo^{sur}$***	***$+H_2O_{ads}$***	***TS2''***	***5H****	***TS3''***	***$3H*+H_2$***
-4%	-0.54	0.81		0.25	0.88	1.88	1.39		-0.59
-3%	-0.56	0.37		0.12	0.58		0.84	1.54	-0.56
-2%	-1.08	0.08		-0.55	0.18		0.24	1.22	-1.08
0%	-1.60	-0.66		-1.38	-0.53		-0.70	0.55	-1.60
2%	-2.05	-1.26		-1.89	-1.44		-1.70	-0.07	-2.05
4%	-2.69	-2.21		-2.68	-2.18		-2.51	-0.74	-2.68

Table S5. Free energies of reduced states during pathways for the hydrogen production on the ***partially (2H*), fully (4H*)*** and ***excessively (5H*)*** hydroxylated CeO_2(111), under different strain at 1000 K.

Strain	*******	Vo^{sub}	***TS1***	Vo^{sur}	$+H_2O_{ads}$	***TS2***	***2H****	***TS3***	$*+H_2$
-4%	0.00	0.18	1.35	0.67	1.14		0.03	2.47	0.00
-3%	0.00	0.08	0.76	0.48	0.95		-0.23	2.66	0.00
-2%	0.00	0.06	0.75	0.29	0.72		-0.41	2.58	0.00
0%	0.00	-0.31	0.53	-0.19	0.34		-0.78	2.26	0.00
2%	0.00	-0.62	0.01	-0.67	-0.04		-1.15	2.13	0.00
4%	0.00	-0.72	-0.56	-1.19	-0.36		-1.52	1.91	0.00
Strain	***3H****	$3H^*+Vo^{sub}$	***TS1'***	$3H^*+Vo^{sur}$	$+H_2O_{ads}$	***TS2'***	***4H****	***TS3'***	$2H^*+H_2$
-4%	-0.12	1.21		0.64	1.38		-0.26	2.48	0.03
-3%	-0.14	0.77		0.52	1.08		-0.58	2.41	-0.23
-2%	-0.67	0.47		-0.16	0.68		-0.92	2.07	-0.41
0%	-1.19	-0.27		-0.99	-0.04		-1.58	1.51	-0.78
2%	-1.64	-0.87		-1.50	-0.95		-2.25	0.98	-1.15
4%	-2.28	-1.81		-2.29	-1.68		-2.89	0.43	-1.52
Strain	***3H****	$3H^*+Vo^{sub}$	***TS1'***	$3H^*+Vo^{sur}$	$+H_2O_{ads}$	***TS2''***	***5H****	***TS3''***	$3H^*+H_2$
-4%	-0.12	1.21		0.64	1.38	2.38	2.08		-0.12
-3%	-0.14	0.77		0.52	1.08		1.54	2.24	-0.14
-2%	-0.67	0.47		-0.16	0.68		0.93	1.91	-0.71
0%	-1.19	-0.27		-0.99	-0.04		-0.01	1.24	-1.19
2%	-1.64	-0.87		-1.50	-0.95		-1.00	0.63	-1.64
4%	-2.28	-1.81		-2.29	-1.68		-1.82	-0.05	-2.26

Table S6. Free energies of reduced states during pathways for the hydrogen production on the ***partially (2H*), fully (4H*)*** and ***excessively (5H*)*** hydroxylated CeO_2(111), under different strain at 1200 K.

Strain	*****	***Vo^{sub}***	***TS1***	***Vo^{sur}***	***$+H_2O_{ads}$***	***TS2***	***2H****	***TS3***	***$*+H_2$***
-4%	0.00	0.13	1.30	0.62	1.58		0.34	2.78	0.00
-3%	0.00	0.03	0.71	0.43	1.39		0.08	2.97	0.00
-2%	0.00	0.01	0.70	0.24	1.16		-0.11	2.88	0.00
0%	0.00	-0.36	0.48	-0.23	0.78		-0.47	2.57	0.00
2%	0.00	-0.67	-0.04	-0.72	0.40		-0.84	2.44	0.00
4%	0.00	-0.77	-0.61	-1.23	-2.92		-1.21	2.22	0.00
Strain	***3H****	***$3H*+Vo^{sub}$***	***TS1'***	***$3H*+Vo^{sur}$***	***$+H_2O_{ads}$***	***TS2'***	***4H****	***TS3'***	***$2H*+H_2$***
-4%	0.33	1.62		1.05	2.28		0.35	3.09	0.34
-3%	0.32	1.17		0.92	1.98		0.03	3.02	0.08
-2%	-0.21	0.88		0.25	1.58		-0.31	2.68	-0.11
0%	-0.73	0.14		-0.58	0.86		-0.97	2.12	-0.47
2%	-1.18	-0.46		-1.09	-0.05		-1.64	1.59	-0.84
4%	-1.82	-1.41		-1.88	-0.79		-2.28	1.04	-1.21
Strain	***3H****	***$3H*+Vo^{sub}$***	***TS1'***	***$3H*+Vo^{sur}$***	***$+H_2O_{ads}$***	***TS2''***	***5H****	***TS3''***	***$3H*+H_2$***
-4%	0.33	1.62		1.05	2.28	3.28	2.84		0.33
-3%	0.32	1.17		0.92	1.98		2.30	3.00	0.32
-2%	-0.21	0.88		0.25	1.58		1.69	2.67	-0.21
0%	-0.73	0.14		-0.58	0.86		0.76	2.01	-0.73
2%	-1.18	-0.46		-1.09	-0.05		-0.24	1.39	-1.18
4%	-1.82	-1.41		-1.88	-0.79		-1.05	0.72	-1.81

Table S7. ΔG_H, E_a and the free energy span required for the WSR on ***partially (2H*), fully (4H*)*** and ***excessively (5H*)*** hydroxylated CeO_2(111), respectively, at 800, 1000 and 1200 K.

T=800 K Strain	**2H***			**4H***			**5H***		
	ΔG_H	E_a	E_{total}	ΔG_H	E_a	E_{total}	ΔG_H	E_a	E_{total}
-4%	0.57	2.44	3.01	0	2.74	2.74	2.69	0	***2.69***
-3%	0.63	2.89	3.52	0	2.99	2.99	1.98	0.70	***2.68***
-2%	0.78	2.99	3.77	0	2.99	2.99	1.71	0.98	***2.69***
0	1.08	3.04	4.12	0	3.09	3.09	1.44	1.25	***2.69***
2%	1.38	3.28	4.66	0	3.23	3.23	1.11	1.63	***2.74***
4%	1.65	3.43	5.08	0	3.32	3.32	0.94	1.77	***2.71***
T=1000 K Strain	**2H***			**4H***			**5H***		
	ΔG_H	E_a	E_{total}	ΔG_H	E_a	E_{total}	ΔG_H	E_a	E_{total}
-4%	0.29	2.44	***2.73***	0	2.74	2.74	2.84	0	2.84
-3%	0.35	2.89	3.24	0	2.99	2.99	2.12	0.70	***2.82***
-2%	0.50	2.99	3.49	0	2.99	2.99	1.85	0.98	***2.83***
0	0.81	3.04	3.85	0	3.09	3.09	1.58	1.25	***2.83***
2%	1.10	3.28	4.38	0	3.23	3.23	1.25	1.63	***2.88***
4%	1.37	3.43	4.80	0	3.32	3.32	1.07	1.77	***2.84***
T=1200 K Strain	**2H***			**4H***			**5H***		
	ΔG_H	E_a	E_{total}	ΔG_H	E_a	E_{total}	ΔG_H	E_a	E_{total}
-4%	0.13	2.44	***2.57***	0.35	2.74	3.09	3.28	0	3.28
-3%	0.03	2.89	***2.92***	0.03	2.99	*3.02*	2.30	0.70	***3.00***
-2%	0.20	2.99	3.19	0	2.99	2.99	2.00	0.98	***2.98***
0	0.50	3.04	3.54	0	3.09	3.09	1.73	1.25	***2.98***
2%	0.80	3.28	4.08	0	3.23	3.23	1.40	1.63	***3.03***
4%	1.07	3.43	4.50	0	3.32	3.32	1.23	1.77	***3.00***

Table S8. Formation energy of creating one oxygen vacancy in the subsurface $E(V_O^{sub})$ of $CeO_2(111)$, at -4%, -3%, -2%, 0, 2%, and 4% strain with different locations of Ce^{3+}. Atom numbering refers to Figure S2. NNN and NN represent Ce^{3+} locating next nearest neighbor and nearest neighbor, respectively. The subscripts of "sur" and "sub" represent Ce^{3+} locating in the top surface and subsurface, respectively.

Ce^{3+} locations to the Vo^{sub}	Atomic number of Ce^{3+}	-4%	-3%	-2%	0	2%	4%
NNN_{sur}-NNN_{sub}	(2,6)	2.51	2.32	2.14	1.75	1.41	1.01
NNN_{sur}-NN_{sur}	(1,2)	2.71	2.48	2.25	1.90	1.49	1.08
NNN_{sur}-NN_{sub}	(2,5)	2.84	2.62	2.42	1.95	1.56	1.05
NN_{sur}-NNN_{sub}	(1,6)	2.75	2.33	2.40	2.20	1.69	1.25
NN_{sur}-NN_{sur}	(1,3)	2.73	2.70	2.53	2.23	1.97	1.56
NN_{sur}-NN_{sub}	(1,5)	3.04	2.88	2.68	2.29	2.10	

Table S9. Formation energy of creating one oxygen vacancy in the top surface $E(V_O^{sur})$ of $CeO_2(111)$, at -4%, -3%, -2%, 0, 2%, and 4% strain with different locations of Ce^{3+}. Atom numbering refers to Figure S2.

Ce^{3+} locations to the Vo^{sur}	Atomic number of Ce^{3+}	-4%	-3%	-2%	0	2%	4%
NNN_{sub}-NNN_{sub}	(5,7)	3.22	2.94	2.64	2.11	1.60	
NN_{sur}-NNN_{sur}	(1,2)	3.19	2.95	2.70	2.19	1.68	1.15
NN_{sur}-NN_{sur}	(2,4)	3.22	3.03	2.84	2.37	1.88	1.37
NN_{sur}-NNN_{sub}	(2,7)	3.49	3.19	2.94	2.46	1.93	1.46

REFERENCES

(1) Gopal, C. B.; García-Melchor, M.; Lee, S. C.; Shi, Y.; Shavorskiy, A.; Monti, M.; Guan, Z.; Sinclair, R.; Bluhm, H.; Vojvodic, A.; Chueh, W. C. Equilibrium Oxygen Storage Capacity of Ultrathin $CeO_{2-\delta}$ Depends Non-Monotonically on Large Biaxial Strain. *Nat. Commun.* **2017**, *8*, 15360.

(2) Ganduglia-Pirovano, M. V.; Da Silva, J. L. F.; Sauer, J. Density-Functional Calculations of the Structure of near-Surface Oxygen Vacancies and Electron Localization on $CeO_2(111)$. *Phys. Rev. Lett.* **2009**, *102*, 026101.

(3) Ma, D.; Lu, Z.; Tang, Y.; Li, T.; Tang, Z.; Yang, Z. Effect of Lattice Strain on the Oxygen Vacancy Formation and Hydrogen Adsorption at CeO_2(111) Surface. *Phys. Lett. A* **2014**, *378*, 2570–2575.

(4) Su, Y.-Q.; Filot, I. A. W.; Liu, J.-X.; Tranca, I.; Hensen, E. J. M. Charge Transport over the Defective CeO_2(111) Surface. *Chem. Mater.* **2016**, *28*, 5652–5658.

(5) Li, H.-Y.; Wang, H.-F.; Guo, Y.-L.; Lu, G.-Z.; Hu, P. Exchange between Sub-Surface and Surface Oxygen Vacancies on CeO_2(111): A New Surface Diffusion Mechanism W. *Chem. Comm.* **2011**, *21*, 6105–6107.

(6) Grasselli, R. K. Fundamental Principles of Selective Heterogeneous Oxidation Atalysis. *Top. Catal.* **2002**, *21*, 79–88.

(7) Capdevila-Cortada, M.; López, N. Descriptor Analysis in Methanol Conversion on Doped CeO_2(111): Guidelines for Selectivity Tuning. *ACS Catal.* **2015**, *5*, 6473–6480.

(8) Deshpande, S.; Patil, S.; Kuchibhatla, S. V.; Seal, S. Size Dependency Variation in Lattice Parameter and Valency States in Nanocrystalline Cerium Oxide. *Appl. Phys. Lett.* **2005**, *87*, 133113.

(9) Farra, R.; Wrabetz, S.; Schuster, M. E.; Stotz, E.; Hamilton, N. G.; Amrute, A. P.; Pérez-Ramírez, J.; López, N.; Teschner, D. Understanding CeO_2 as a Deacon Catalyst by Probe Molecule Adsorption and in Situ Infrared Characterisations. *Phys. Chem. Chem. Phys.* **2013**, *15*, 3454–3465.